https://doi.org/10.5194/cp-2020-39
Preprint. Discussion started: 30 March 2020

Climate of the Past Discussions

Large scale climate signals of a European oxygen isotope network from tree-rings - predominantly caused by ENSO teleconnections?

Daniel F. Balting[1], Monica Ionita[1], Martin Wegmann[1], Gerhard Helle[2], Gerhard H. Schleser[3], Norel Rimbu[1], Mandy B. Freund[4,5], Ingo Heinrich[2,6], Diana Caldarescu[1] & Gerrit Lohmann[1,7]

[1]Alfred Wegener Institute, Bremerhaven, 27570, Germany
[2]German Research Centre for Geosciences, Potsdam, 14473, Germany
[3]IBG-3, Forschungszentrum Jülich, 52428, Germany
[4]Climate and Energy College, University of Melbourne, Melbourne, 3010, Australia
[5]CSIRO Agriculture and Food, Melbourne, Australia
[6]Geography Department, Humboldt University, Berlin, 10099, Germany
[7]Physics Department, University of Bremen, Bremen, 28359, Germany

Correspondence to: Daniel F. Balting (daniel.balting@awi.de)

Abstract. We investigate the annual variability of $\delta^{18}O$ tree ring records from sites distributed all over Europe covering the last 400 years. An Empirical Orthogonal Function (EOF) analysis reveals two distinct modes of variability on the basis of the existing $\delta^{18}O$ tree ring records. The first mode of $\delta^{18}O$ variability is associated with anomaly patterns of the El Niño-Southern Oscillation (ENSO) and reflects a multi-seasonal climatic signal. The ENSO signal is visible for the last 130 years, but is found weak during the period 1600 to 1850 suggesting that the relationship between ENSO and the European climate may not stable over time. The second mode of $\delta^{18}O$ variability, which captures an out-of-phase variability between northwestern and southeastern European $\delta^{18}O$ tree ring records, is related to a regional summer atmospheric circulation pattern revealing a pronounced centre over the North Sea. Locally, the $\delta^{18}O$ anomalies associated with this mode show the same (opposite) sign with temperature (precipitation). We infer that the investigation of large-scale atmospheric circulation patterns and related teleconnections far beyond instrumental records can be done with oxygen isotopic signature derived from tree rings. However, the European $\delta^{18}O_{cel}$ tree network needs to be consolidated and updated, as well as additional research on the stationarity of reconstructed climate signals and the stationarity of teleconnections is advisable.

1 Introduction

Vegetation cover is a key component of the global climate system and forest trees represent a substantial part of it. Tree growth is irrevocably affected by interactions with hydrosphere, atmosphere, and pedosphere and the influence of environmental factors is stored in the physical and chemical properties of each tree ring (Schweingruber, 1996). A major component of a tree ring is cellulose, which consists of the elements carbon, oxygen and hydrogen. Their stable isotope signatures are determined by varying environmental conditions influencing a series of fractionation processes during the uptake of CO_2 and H_2O from atmosphere and soil and biosynthesis of tree-ring cellulose. For instance, the climate signature

https://doi.org/10.5194/cp-2020-39
Preprint. Discussion started: 30 March 2020


Climate of the Past Discussions

of $\delta^{13}C$ values of tree-ring cellulose basically originates from fractionations during photosynthesis at the leaf or needle level that generally lower the $\delta^{13}C$ of the atmospheric CO_2 source which contains no direct climatic signal (Schleser, et al. 1995). $\delta^{18}O$ of tree-ring cellulose ($\delta^{18}O_{cel}$) is of particular interest for paleoclimate studies because it is related to source water, i.e. $\delta^{18}O$ of precipitation ($\delta^{18}O_P$), which is directly affected by climate processes, i.e. temperature during droplet condensation within air masses, transport distance from ocean source, type of precipitation (e.g. rain or snow) and precipitation amount (e.g. Dansgaard, 1964; Epstein et al., 1977; Rozanski et al., 1993). Within the arboreal system, $\delta^{18}O$ of soil water ($\delta^{18}O_{SW}$) constitutes the $\delta^{18}O$ input and usually represents an average $\delta^{18}O_P$ over several precipitation events modified by partial evaporation from the soil (depending on soil texture and porosity) and by a possible time lag, depending on rooting depth (Saurer et al., 2012). Representing the baseline variability, $\delta^{18}O_{SW}$ is invariably tied to the oxygen isotope signature of tree-ring cellulose ($\delta^{18}O_{cel}$).

However, $\delta^{18}O_{cel}$ is dependent on two more clusters of fractionations that reflect tree-internal processes, namely evaporative ^{18}O-enrichment of leaf or needle water via transpiration, and biochemical fractionations including partial isotopic exchange of cellulose precursors with trunk water during cellulose biosynthesis (e.g. Saurer et al., 1997; Roden et al., 2000; Barbour, 2007; Kahmen et al., 2011; Treydte et al., 2014 and citations therein). The biochemical fractionation during cellulose biosynthesis can be largely considered as constant (27 ±4‰ (Sternberg and DeNiro, 1983)); however, varying leaf-to-air vapour pressure deficit following varying air humidity causes corresponding changes in the $\delta^{18}O$ signature of leaf or needle water (e.g.Helliker and Griffiths (2007)). Although modified and dampened by physiological processes (e.g. Pèclet effect (Farquhar and Lloyd, 1993) and oxygen isotope exchange with stem water during cellulose synthesis (Hill et al., 1995)) variability of ^{18}O enrichment of leaf-water is clearly affecting $\delta^{18}O_{cel}$, besides the strong signature of $\delta^{18}O_P$. For example, the $\delta^{18}O_{cel}$ are used to reconstruct precipitation (e.g. Rinne et al., 2013), air temperature (e.g. Porter et al., 2014) and drought (e.g. Nagavciuc et al., 2019). Since these quantities are largely based on transport processes within the atmosphere, the $\delta^{18}O_{cel}$ values can be used to get detailed information about large-scale atmospheric circulation patterns (Andreu-Hayles et al., 2017; Trouet et al., 2018, Nagavciuc et al., 2019). The resulting long-term perspective can be the key to identify the influence of different external forcing on, and internal variability of the behavior of large-scale atmospheric circulation.

One of the most important components for the internal climate variability is the El Niño – Southern Oscillation (ENSO) which influences the atmospheric circulation globally (Allan, 1996). Since the ENSO variability is strongest in winter, multiple studies have identified a significant ENSO impact on the European climate during this season. Observational studies (Fraedrich and Müller, 1992; Fraedrich, 1994; Pozo-Vazquez, 2005; Brönnimann, 2004; Brönnimann, 2007) and model studies (Merkel and Latif, 2002; Mathieu et al., 2004) suggest that an El Niño event leads to a negative phase of the North Atlantic Oscillation (NAO) with cold and dry conditions over Northern Europe and wet and warm conditions over Southeastern Europe in winter. Furthermore, it is also possible to identify a significant ENSO influence with regard to European precipitation in spring (Brönnimann, 2007; Lloyd-Hughes and Saunders, 2002; Helama et al., 2009). However, significant impacts of ENSO regarding European droughts could only be detected for the most extreme El Niño events (King

https://doi.org/10.5194/cp-2020-39
Preprint. Discussion started: 30 March 2020


Climate of the Past Discussions

et al., 2020). To what extent these preconditions influence the climate conditions during summer is not yet known for Europe, but it can serve as a key for a better understanding of European climate. However, the relatively short period of existing instrumental data (van Oldenburgh and Burgers, 2005; Brönnimann, 2007), makes it difficult to describe the full range of ENSO variability and its possible consequences for the climate of the European continent (Domeisen et al., 2019).

The aim of this study is to present a comprehensive spatiotemporal analysis of the large-scale European atmospheric circulation based on the influence of the ENSO variability over a long-term perspective. This study is based on the climatological signals of a European $\delta^{18}O_{cel}$ network. For this purpose, Section 2 characterizes the isotope network. The used climate data and methods are described in this Section as well. The results in Section 3 concentrate on the fundamental description of the dataset (Sect. 3.1) and the combined climate signal of the network (Sect 3.2). The links to ENSO are investigated using a multi seasonal perspective with different statistical approaches in Section 3.3. The multi seasonal signals of the $\delta^{18}O_{cel}$ in combination with modelled $\delta^{18}O_P$ and $\delta^{18}O_{SW}$ are presented in Section 3.4. Furthermore, the second strongest climate signal is shortly introduced in Section 3.5. The final section summarizes the major results.

2 Data and Methods

2.1 The isotope network

We investigate the dominant modes of variability of 26 $\delta^{18}O_{cel}$ records, distributed over Europe, and their relationships with regional and large-scale climate anomalies. 22 of the 26 $\delta^{18}O_{cel}$ records were created within the EU project ISONET (Annual Reconstructions of European Climate Variability using a High-Resolution Isotopic network) (Treydte et al., 2007a, b). Furthermore, four additional sites from Bulgaria, Turkey, Southwest Germany and Slovenia were added (Hafner et al., 2014; Heinrich et al., 2013). In total, the isotope network contains eight broadleaf tree sites (*Quercus*) and 18 coniferous tree sites (*Pinus, Juniper, Larix, Cedrus*) from altitudes varying for each location from 10m up to 2200m above sea level (Fig. 1). 24 of the 26 sites are distributed over the European continent whereas two additional sites are located in the Atlas Mountains of Morocco and in the Taurus Mountains of Turkey.

The stable isotopes of oxygen in tree-ring cellulose, reported as $\delta^{18}O_{cel}$ vs. SMOW (Craig, 1957) of each site were determined as described by Treydte et al. (2007a, b). At least four dominant trees were chosen per site and two increment cores were taken per tree. After the standard dendrochronological dating following Fritts (1976), the individual tree rings were dissected from the cores. However, for oak only the latewood was used for the analyses. This procedure assumed that climate signals of the current year were predominantely applied since early wood of oaks frequently contains climate information of the preceding year (Hill et al., 1995). The temporal resolution of the isotope records is annually.

The first 100 years of data from the network as well as a general description have already been published (Treydte et al., 2007a, b). Data from individual sites or regional groups of sites where published elsewhere (Andreu-Hayles et al., 2017;

https://doi.org/10.5194/cp-2020-39
Preprint. Discussion started: 30 March 2020

Etien et al., 2009; Haupt et al., 2011; Helama et al., 2014; Hilasvuori et al., 2009; Labuhn et al., 2014; Labuhn, et al., 2016; Rinne et al., 2013; Saurer et al., 2008; Saurer et al., 2012; Saurer et al., 2014; Vitas, 2008). Here, here we use the extended ISONET+ product with the longest chronologies cover a period from 1600 to 2005. The highest data density is available for the period 1850-1998 with 26 time series available for further analysis. 12 time series cover the entire period of 400 years.

2.2 Climate data

We use the gridded fields of the 20th Century Reanalysis Project (20CR) version V2c (Compo et al., 2011) for the climatological analysis. The 20CR version V2c covers the period from 1851-2014 and has a temporal resolution of six hours and a spatial resolution of 2°×2°. Additionally, the reanalysis data of the Global Precipitation Climatology Centre (GPCC; Schneider et al., 2014) is used to study the relationship between the $\delta^{18}O_{cel}$ and the precipitation anomalies. Furthermore, the COBE-SST2 dataset (Hirahara et al., 2014) is included in the study. To identify the links to drought conditions in Europe we make use of the Standardized Precipitation Evapotranspiration Index (SPEI3) dataset (Vicente-Serrano et al., 2010).
The data from both reanalyses were seasonally averaged: DJF (December to February), MAM (March to May), JJA (June to August) and SON (September to November). Since we focus on interannual to decadal variability, the linear trends from each grid cell have been removed.

2.3 Nudged model scenarios

Beside the observational/reanalysis-based climate data, we also investigate the relation between $\delta^{18}O_P$ and $\delta^{18}O_{SW}$ to receive further insights about the fractionation / photosynthesis processes. Here, we analyse modelled data based on nudged ECHAM5-wiso simulations with ERA-40 and ERA-Interim reanalysis fields (Uppala et al., 2005; Berrisford et al., 2011; Dee et al., 2011) for the period 1960 to 2005 for the European region (Butzin et al., 2014).

2.4 Data analysis

As a first step, the characteristics of each time series of the $\delta^{18}O_{cel}$ network and their relation to altitude and latitude are investigated. For a better comparison, the linear trend of each $\delta^{18}O_{cel}$ time series are removed and all time series are standardized (z-values).
To combine the signals of the isotope network, we use the Principle Component Analysis (PCA) and the Empirical Orthogonal Functions (EOF). These techniques were described by Pearson (1902) and Hotteling (1935) and were used for the first time by Lorenz (1956) for climatological studies (Storch and Zwiers, 1999). The EOFs are used to identify the most dominant patterns of the $\delta^{18}O_{cel}$ tree network variability. By applying the PCA, it is possible to gain a temporal perspective of these patterns since the phase and amplitude are described by the principal components (PC). In addition, the final components are checked if they can be analysed meaningfully by the rule of Kaiser (1960), which indicates that the

https://doi.org/10.5194/cp-2020-39
Preprint. Discussion started: 30 March 2020


Climate of the Past Discussions

eigenvalue (λ) of a component has to be λ> 1. The following components are further checked if they fulfil the requirements of the rule of North et al. (1982). This rule states that the pattern of the eigenvectors of one component is strongly contaminated by other EOFs that correspond to the closest eigenvalues (Storch and Zwiers, 1999).

The ISONET network consists of a multi-site and multi-species tree-ring network covering more or less the period between 1600 to 2003. However, some tree-ring series cover the whole period, others cover only a shorter period. In order to be able to have a long-term perspective, one needs to find a statistically meaningful way to extend the shorter records to make use of the whole 400 years of data. Since most Multilinear Principal Component Analysis algorithms do not work with gaps in the initial matrix we make use of an algorithm developed by Josse and Husson (2016) which is able to fill the temporal gaps without a change of the PC. In the first step we place the mean in the gap and execute a PCA with this dataset. Afterwards, the dataset is projected onto the new component axis. So, that the values are rotated and the value of a gap change. The new value for the gap is placed into the initial dataset. With this new dataset, a PCA is again carried out. This process is repeated until convergence is reached. The result is a gap-free dataset which can be used for PCA.

Composite maps of observed precipitation, air temperature, geopotential height 500mb (Z500) and SST are defined by extreme values of the network's principle component above a certain threshold. We choose events above and below one standard deviation with respect to the mean. The average climate conditions expressed by the composites allow us to analyse the general climate state occurring at times of extreme minima or maxima separately. In addition, both composites of climate conditions are combined under the assumption that the extremes of the minima and maxima show exactly the opposite climate state. For this purpose, the minimum composite is subtracted from the maximum composite at each grid point.

Beside the composite maps, we extract the values of PC1 for those years for which ENSO values are higher than the average plus one standard deviation and lower than the average minus one standard deviation. The difference from the former distribution for the values of minima and maxima years is tested with the t-test. To better understand if El Niño or La Niña events coeval with extremes in the $\delta^{18}O_{cel}$ time series, the Event Coincidence Analysis (Siegmund et al., 2017; Donges et al., 2016) using the PC1 and a December Nino 3.4 index is applied (HadISST1; Rayner et al., 2003). Therefore, we analyze whether the years in which the Nino 3.4 index is above the 75th percentile match the 75th percentile in PC1. In general, a significance level of α= 0.05 was used in all analyses.

Finally, we analyse the relation between seasonally averaged $\delta^{18}O_P$ and $\delta^{18}O_{SW}$ from winter, spring and summer, based on nudged ECHAM5-wiso simulations (Butzin et al., 2014), with PC1 based on the $\delta^{18}O_{cel}$ values from the ISONET network.

3 Results and Discussion

3.1 Characteristics of the $\delta^{18}O_{cel}$ network

The data distribution of each time series is shown in a boxplot diagram to give an overview of the characteristics of the isotope network (Fig. 2A). The individual sites are primarily ordered for tree types and afterwards ordered in ascending order

https://doi.org/10.5194/cp-2020-39
Preprint. Discussion started: 30 March 2020


Climate of the Past Discussions

by their means. The highest mean $\delta^{18}O_{cel}$ values occur at the southern locations, i.e. in Turkey and Carzola in Spain. For oaks and pines, the lowest mean values are found for the northern sites. Moreover, generally lower $\delta^{18}O_{cel}$ values are identified for *Quercus* compared to *Pinus*. This might be determined genetically, because also $\delta^{13}C_{cel}$ values of angiosperms co-occurring with gymnosperms are typically found more negative. Angiosperm wood tissue contains vessels, i.e. specialized water-conducting cells that are generally larger in diameter, and therefore more conductive to water, than conifer wood cells (Sperry et al., 2006).

The overall variance of the datasets is not dependent on the type of tree species. The highest scattering is found for the $\delta^{18}O_{cel}$ time series from Poellau in Austria, whereas the lowest standard deviation is identified for the time series from Lochwood in Great Britain.

Since the $\delta^{18}O$ source values and the fractionation processes are temperature dependent, it is necessary to evaluate the influence of altitude and latitude for the oxygen isotope ratio. The relation of the $\delta^{18}O_{cel}$ values with regard to altitude and latitude of each site is shown in Figs. 2B and 2C. In Fig. 2C, the linear relationship between the average $\delta^{18}O_{cel}$ values of the locations and the corresponding latitudes are plotted. As shown by the boxplots of Fig. 2A, southern sample sites are characterized by the highest average $\delta^{18}O_{cel}$ values whereas northern sites show the lowest average $\delta^{18}O_{cel}$ values. The relation between the $\delta^{18}O_{cel}$ values and latitude is yielding a significant linear regression.

Beside the latitudinal effect, altitude also influences the oxygen isotope ratios as shown in Fig. 2B which can likewise be described by a linear regression. It should be noted, that the southern sites are found at higher altitudes than the northern sites, which could influence the relation by a latitudinal effect. Therefore, we show that the $\delta^{18}O_{cel}$ network is influenced by a latitudinal and an altitudinal effect, thereby supplying a proof of concept for the often-stated effects of latitude, altitude and continentality on the isotopic source value of water (McCarroll and Loader, 2004).

3.2 Characteristics of the principal components

Performing PC analyses, the first component of the isotope network explains 16.2%, the second 9.1%, the third 6.4%, the fourth 5.5%, and the fifth 5.2% of the variance. Therefore, the first five components explain a cumulative variability of around 43%. Concerning the rule of Kaiser (1960), the first nine components can thus be meaningfully analysed. Since the first two components also fulfilled the requirements of the rule of North et al. (1982), they are investigated by their temporal and spatial characteristics.

The dominant pattern (EOF1), which describes 16.2% of the total variance, shows a spatially homogeneous pattern (Fig. 3A). The majority of time series in Europe are characterized by negative eigenvectors. The pole of this EOF pattern is centred over France and Germany. In contrast, tree sites close to the Mediterranean Sea and the northernmost site in Finland are characterized by eigenvectors close to zero. Therefore, these locations contribute little to the first component's time series (PC1) shown in Fig. 3C.

https://doi.org/10.5194/cp-2020-39
Preprint. Discussion started: 30 March 2020


Climate of the Past Discussions

The second EOF (EOF2) is characterized by a completely different spatial pattern (Fig. 3B). Negative eigenvectors are found around the North and Baltic Sea, with the smallest eigenvector located in Norway. Positive eigenvectors are identified especially for Southern/Southeast Europe and the Alps. The highest eigenvectors are recorded for the Italian site. In summary, this component highlights a dipole-like structure between Northern and Southern/Southeast Europe. The time series of the second component (PC2) shows a tendency towards higher values from the mid of the 19th century onwards. Furthermore, the highest interannual variability is found for the beginning of the 18th and 19th century. The highest values of the second component (PC2) are reached at the beginning of the 18th century, whereas the smallest values are identified for the beginning of the 19th century (Fig. 3 D).

3.3 Links between ENSO and PC1

For the winter season, positive values of PC1 are associated with a warm (cold) Pacific around the Equator and warm (cold) temperatures on the west coast of North and South America. This signal persists from winter (Fig 4A), throughout spring (Fig 4B) into summer (Fig 4C) and indicates that positive (negative) values of summer PC1 are co-evolving with the occurrence of El Niño (La Niña) conditions. The related large-scale atmospheric circulation is shown in the composite map of Z500 (third row of Figure 4). For the winter season (Figure 4 D), a deep (weak) Aleutian Low and a positive (negative) mode of the Pacific-North America Pattern (PNA; Wallace and Gutzler, 1981) are observed, which are often associated with the occurrence of El Niño (La Niña) events (Pozo-Vázquez et al., 2001). The strong (weak) Aleutian Low, the low-pressure (high-pressure) regime over Europe and strengthened (weaker) high-pressure regime in northern high-latitudes correspond to a negative (positive) phase of the Arctic Oscillation (AO). Since the AO characterizes the variability of storm tracks in the Northern Hemisphere, a shift of the storm track during El Niño and La Niña was recognized in surface pressure, temperature and precipitation (Fraedrich, 1994; Fraedrich and Müller, 1992).

Furthermore, a negative phase of the winter NAO is also visible in the composite maps with cold and dry conditions over Northern Europe and wet and warm conditions over Southeastern Europe. In addition to elevated near surface temperature anomalies over Europe, the El Niño signal is visible in northern hemispheric temperature anomalies (Ineson and Scaife, 2008). That is also visible in density plots of PC1 (Supp. 1), which show that during El Niño years, the distribution of the PC1 is shifted towards higher values, whereas the distribution of the PC1 is shifted towards lower values for La Niña years. According to the t-test, both shifts are significantly different ($p < 0.05$).

In composite maps for spring (Fig. 4B, 4E, 4H, 4K), the atmospheric circulation remains in a similar configuration over Europe and the North Atlantic compared to the winter season. In contrast, the equatorial Atlantic and the coast of South America show an enhanced warming (cooling) signal. A lagged warming of the equatorial Atlantic is identified up to 6 months after an El Niño event (Latif and Grötzner, 1999).

Based on consistent climate conditions during winter and spring in the European mid latitudes, the summer climate is influenced by background hydroclimate preconditions (Fig. 4C, 4F, 4I, 4L). The European climate is characterized by higher

https://doi.org/10.5194/cp-2020-39
Preprint. Discussion started: 30 March 2020


Climate of the Past Discussions

(lower) precipitation in Central Europe as well as lower (higher) surface air temperatures in summer corresponding to low (high) $\delta^{18}O_{cel}$ values. Furthermore, the Northeast Atlantic shows cold (warm) temperatures whereas the North Atlantic south of Greenland shows a warming (cooling) tendency. This particular SST anomaly pattern is often associated with droughts and heatwaves in Europe (Feudale and Shukla, 2011; Ionita et al., 2017).

To test if there is a significant relationship between the variability of our $\delta^{18}O_{cel}$ records and drought variability, we correlated the JJA PC1 time series with the Central Europe JJA SPEI3 drought index (Vicente-Serrano et al., 2010; Longitude -5° to 10°/Latitude 46° to 52°). The SPEI3 index is suitable for this analysis because we to take into account the climate conditions of the pre-season to make it comparable to PC1. For the period from 1901 to 2005, the correlation is significant ($R=0.49$; $p < 0.01$). To better understand whether extremes in $\delta^{18}O_{cel}$ time series co-occurring with El Niño or La Niña events, we apply the Event Coincidence Analysis (Siegmund et al., 2017; Donges et al., 2016) using PC1 and December Nino 3.4 index (HadISST1; Rayner et al., 2003). Over the period 1871-2005, 41.2% of the Nino 3.4 high and low extremes coincided significantly during winter, with high and low extremes of PC1 ($p < 0.01$). Extending the period from 1600 to 2005, the used reconstruction (Dätwyler et al., 2019) and other ENSO reconstructions (Freund et al., 2019; Li et al., 2011), show that the correlations and coincidence rates are weakening (not shown), which indicates that the relationship between PC1 and ENSO might not be stable over time.

3.4 Comparison of $\delta^{18}O_{cel}$ with modelled $\delta^{18}O$ in precipitation and soil water

By employing nudged climate simulations with ECHAM5-wiso (Butzin et al., 2014), we aim at gaining better insight into how well the $\delta^{18}O_{cel}$ tree signature is able to capture a multi-seasonal signal. A significant correlation between PC1 and $\delta^{18}O_P$ is shown in the correlation maps for winter, spring and summer, where Central Europe is characterized by a moderate correlation (Fig. 6). A similar pattern can be identified for the correlation between $\delta^{18}O_{SW}$ and PC1. Compared to our previous analysis, the correlation between these quantities is increasing from winter to summer where it reached the maximum correlation. Since the $\delta^{18}O_{cel}$ ratio is largely dependent on the isotopic composition of soil water, the correlation is even stronger with the $\delta^{18}O_P$. We suggest that the $\delta^{18}O_{cel}$ signal is a multi-seasonal signal which captures the hydroclimatic conditions from winter towards summer. The reason for this situation is that depending on the root system, winter snowfall and groundwater storage, trees use water from previous seasons for photosynthesis (Treydte et al., 2006). Additionally, it is thereby implied that the duration of the water uptake should also be considered (Tang and Feng, 2001).

3.4 Further climate signals in $\delta^{18}O_{cel}$

Besides the multi-seasonal signal, the second component of the $\delta^{18}O_{cel}$ values significantly relates to the summer climate (Fig. 5). The second EOF of the $\delta^{18}O_{cel}$ values, which explains 9.5 % of the total variance, shows a dipole-like pattern between northern and south-eastern Europe (Fig. 3B). This phenomenon is strongly visible in all composite maps (Fig. 5) and known as the dominant summer atmospheric circulation of the European climate (Casty et al., 2007). A positive

https://doi.org/10.5194/cp-2020-39
Preprint. Discussion started: 30 March 2020


Climate of the Past Discussions

(negative) geopotential height anomaly in northern Europe co-occurs with a negative (positive) Z500 anomaly in southeastern Europe. The positive geopotential height anomaly is often described as atmospheric blocking-like pattern which is related to climate extremes like floods and droughts for European mid-latitudes (Sillmann and Croci-Maspoli, 2009). Moreover, this circulation anomaly pattern has been identified as the primary driver for extreme dry periods over the Eastern Mediterranean (Oikonomou et al., 2010) as well as the dominant driver for summer air temperature variability in Greece (Xoplaki et al., 2003a, b).

The temporal distribution of extremes in the PC2 time series, indicates that the 19th century has experienced increased drought in northern Europe and enhanced precipitation in the Adriatic region (Fig. 3D). In addition, climate reconstructions also indicate that the Central part of Europe and parts of southern Sweden were relatively dry during the 19th century (Seftigen et al., 2013; Hanel et al., 2018). Since temperature extremes and precipitation patterns are largely determined by atmospheric blocking activity in these latitudes (Pfahl and Wernli, 2012), we suggest that the drought like conditions in northern Europe during summer are based on an enhanced atmospheric blocking activity.

4 Summary and conclusions

We present a $\delta^{18}O_{cel}$ isotope network from tree rings for the last 400 years which was used to investigate the large-scale climate signals in the European mid-latitudes. According to our analysis, the climate signals of the network indicate a relation exists for winter, spring and summer with ENSO. The nudged model suggests that the summer signal is still dominating $\delta^{18}O_{cel}$ but is partly influenced by lagged winter and spring signals. We argue that this is based on hydroclimatic feedback processes as well as characteristics of the water reservoirs of the different sample sites. The ENSO signal is clearly visible for the last 130 years. However, no significant links can be deduced during the period 1600 to 1850 which is indicating that the relationship between ENSO and the European climate is not stable over time. The teleconnection changes between the tropical Pacific and Europe during the pre-instrumental period were also identified by other climate proxies (Rimbu et al., 2003).

Furthermore, our study shows the second mode with a dipole between North and Southeast Europe. Since this mode is highly relevant for the summer climate conditions on the entire European continent, the temporal perspective gives new insights about how the frequency of this mode changed through time. Our findings suggest that there is a tendency towards a situation whereby Southeast Europe is predominantly characterized by a high-pressure system and North Europe by a low-pressure system starting at the beginning of the 20th century.

Future research is required to provide additional insights into the stationarity of reconstructed climate signals and also the stationarity of teleconnections. Moreover, the European $\delta^{18}O_{cel}$ tree network needs to be updated to capture the climate changes of the last 15 years. In addition, it is imperative to extent the isotope network by collecting more $\delta^{18}O_{cel}$ records from Eastern Europe to improve the validity of our results for this region. In the context of the ongoing discussion about the

https://doi.org/10.5194/cp-2020-39
Preprint. Discussion started: 30 March 2020

anthropogenic climate change, stable isotope records can provide useful information about the perturbed and unperturbed large-scale atmospheric circulation patterns.

Acknowledgement

D.B. and D.C. are funded by the PalEX Project (AWI Strategy Fund) and M.I. is funded by the REKLIM project. All but four tree-ring stable isotope chronologies were established within the project ISONET supported by the European Union (EVK2-CT-2002-00147 'ISONET'). We want to thank all participants of the ISONET project (L. Andreu, Z. Bednarz, F. Berninger, T. Boettger, C. M. D'Alessandro, J. Esper, N. Etien, M. Filot, D. Frank, M. Grabner, M. T. Guillemin, E. Gutierrez, M. Haupt, E. Hilasvuori, H. Jungner, M. Kalela-Brundin, M. Krapiec, M. Leuenberger, H.H. Leuschner, N. J. Loader, V. Masson-Delmotte, A. Pazdur, S. Pawelczyk, M. Pierre, O. Planells, R. Pukiene, C. E. Reynolds-Henne, K. T. Rinne, A. Saracino, M. Saurer, E. Sonninen, M. Stievenard, V. R. Switsur, M. Szczepanek, E. Szychowska-Krapiec, L. Todaro, K. Treydte, J. S. Waterhouse, and M. Weigl). The data from Turkey, Slovenia and Southwest Germany were produced with the EU-funded project MILLENNIUM (GOCE 017008-2'MILLENNIUM'), special thanks to T. Levanic and R. Touchan. The tree-ring stable isotope chronologies from Bulgaria were established with support of the German Research Foundation DFG (HE3089-1, GR 1432/11-1) and in cooperation with the administration of Pirin National Park, Bulgaria. Additionally, we want to thank M. Butzin and M. Werner for providing the $\delta^{18}O$ in precipitation and $\delta^{18}O$ of the soil water from nudged ECHAM5-wiso simulations.

References

Allan, R. J., Lindesay, J. and Parker, D. E.: El Niño, southern oscillation & climatic variability, CSIRO, Collingwood, Vic., Australia., 1996.

Andreu-Hayles, L., Ummenhofer, C. C., Barriendos, M., Schleser, G. H., Helle, G., Leuenberger, M., Gutiérrez, E. and Cook, E. R.: 400 Years of summer hydroclimate from stable isotopes in Iberian trees, Clim Dyn, 49(1–2), 143–161, doi:10.1007/s00382-016-3332-z, 2017.

Barbour, M. M.: Stable oxygen isotope composition of plant tissue: a review, Functional Plant Biol., 34(2), 83–94, doi:10.1071/FP06228, 2007.

Berrisford, P., Kållberg, P., Kobayashi, S., Dee, D., Uppala, S., Simmons, A. J., Poli, P. and Sato, H.: Atmospheric conservation properties in ERA-Interim, Quarterly Journal of the Royal Meteorological Society, 137(659), 1381–1399, doi:10.1002/qj.864, 2011.

https://doi.org/10.5194/cp-2020-39
Preprint. Discussion started: 30 March 2020

Brönnimann, S., Luterbacher, J., Staehelin, J., Svendby, T. M., Hansen, G. and Svenøe, T.: Extreme climate of the global troposphere and stratosphere in 1940–42 related to El Niño, Nature, 431(7011), 971, doi:10.1038/nature02982, 2004.

Brönnimann, S., Xoplaki, E., Casty, C., Pauling, A. and Luterbacher, J.: ENSO influence on Europe during the last centuries, Climate Dynamics, 28(2–3), 181–197, doi:10.1007/s00382-006-0175-z, 2007.

Butzin, M., Werner, M., Masson-Delmotte, V., Risi, C., Frankenberg, C., Gribanov, K., Jouzel, J. and Zakharov, V. I.: Variations of oxygen-18 in West Siberian precipitation during the last 50 years, Atmospheric Chemistry and Physics, 14(11), 5853–5869, doi:10.5194/acp-14-5853-2014, 2014.

Casty, C., Raible, C. C., Stocker, T. F., Wanner, H. and Luterbacher, J.: A European pattern climatology 1766–2000, Climate Dynamics, 29(7–8), 791–805, doi:10.1007/s00382-007-0257-6, 2007.

Compo, G. P., Whitaker, J. S., Sardeshmukh, P. D., Matsui, N., Allan, R. J., Yin, X., Gleason, B. E., Vose, R. S., Rutledge, G., Bessemoulin, P., Brönnimann, S., Brunet, M., Crouthamel, R. I., Grant, A. N., Groisman, P. Y., Jones, P. D., Kruk, M. C., Kruger, A. C., Marshall, G. J., Maugeri, M., Mok, H. Y., Nordli, ø., Ross, T. F., Trigo, R. M., Wang, X. L., Woodruff, S. D. and Worley, S. J.: The Twentieth Century Reanalysis Project, Quarterly Journal of the Royal Meteorological Society, 137(654), 1–28, doi:10.1002/qj.776, 2011.

Craig, H.: Isotopic standards for carbon and oxygen and correction factors for mass-spectrometric analysis of carbon dioxide, Geochimica et Cosmochimica Acta, 12(1–2), 133–149, doi:10.1016/0016-7037(57)90024-8, 1957.

Dansgaard, W.: Stable isotopes in precipitation, Tellus, 16(4), 436–468, doi:10.1111/j.2153-3490.1964.tb00181.x, 1964.

Dee, D. P., Uppala, S. M., Simmons, A. J., Berrisford, P., Poli, P., Kobayashi, S., Andrae, U., Balmaseda, M. A., Balsamo, G., Bauer, P., Bechtold, P., Beljaars, A. C. M., van de Berg, L., Bidlot, J., Bormann, N., Delsol, C., Dragani, R., Fuentes, M., Geer, A. J., Haimberger, L., Healy, S. B., Hersbach, H., Hólm, E. V., Isaksen, L., Kållberg, P., Köhler, M., Matricardi, M., McNally, A. P., Monge-Sanz, B. M., Morcrette, J.-J., Park, B.-K., Peubey, C., de Rosnay, P., Tavolato, C., Thépaut, J.-N. and Vitart, F.: The ERA-Interim reanalysis: configuration and performance of the data assimilation system, Quarterly Journal of the Royal Meteorological Society, 137(656), 553–597, doi:10.1002/qj.828, 2011.

Domeisen, D. I. V., Garfinkel, C. I. and Butler, A. H.: The Teleconnection of El Niño Southern Oscillation to the Stratosphere, Reviews of Geophysics, doi:10.1029/2018RG000596, 2019.

Donges, J. F., Schleussner, C.-F., Siegmund, J. F. and Donner, R. V.: Event coincidence analysis for quantifying statistical interrelationships between event time series, Eur. Phys. J. Spec. Top., 225(3), 471–487, doi:10.1140/epjst/e2015-50233-y, 2016.

Epstein, S., Thompson, P. and Yapp, C. J.: Oxygen and Hydrogen Isotopic Ratios in Plant Cellulose, Science, 198(4323), 1209–1215, doi:10.1126/science.198.4323.1209, 1977.

Etien, N., Daux, V., Masson-Delmotte, V., Mestre, O., Stievenard, M., Guillemin, M. T., Boettger, T., Breda, N., Haupt, M. and Perraud, P. P.: Summer maximum temperature in northern France over the past century: instrumental data versus multiple proxies (tree-ring isotopes, grape harvest dates and forest fires), Climatic Change, 94(3), 429–456, doi:10.1007/s10584-008-9516-8, 2009.

Farquhar, G. D. and Lloyd, J.: 5 - Carbon and Oxygen Isotope Effects in the Exchange of Carbon Dioxide between Terrestrial Plants and the Atmosphere, in Stable Isotopes and Plant Carbon-water Relations, edited by J. R. Ehleringer, A. E. Hall, and G. D. Farquhar, pp. 47–70, Academic Press, San Diego., 1993.

Feudale, L. and Shukla, J.: Influence of sea surface temperature on the European heat wave of 2003 summer. Part I: an observational study, Climate Dynamics, 36(9–10), 1691–1703, doi:10.1007/s00382-010-0788-0, 2011.

Fraedrich, K.: An ENSO impact on Europe?, Tellus A, 46(4), 541–552, doi:10.1034/j.1600-0870.1994.00015.x, 1994.

Fraedrich, K. and Müller, K.: Climate anomalies in Europe associated with ENSO extremes, International Journal of Climatology, 12(1), 25–31, doi:10.1002/joc.3370120104, 1992.

Freund, M. B., Henley, B. J., Karoly, D. J., McGregor, H. V., Abram, N. J. and Dommenget, D.: Higher frequency of Central Pacific El Niño events in recent decades relative to past centuries, Nature Geoscience, doi:10.1038/s41561-019-0353-3, 2019.

Fritts, H.: Tree Rings and Climate, Elsevier., 2012.

Gessler, A., Ferrio, J. P., Hommel, R., Treydte, K., Werner, R. A. and Monson, R. K.: Stable isotopes in tree rings: towards a mechanistic understanding of isotope fractionation and mixing processes from the leaves to the wood, Tree Physiology, 34(8), 796–818, doi:10.1093/treephys/tpu040, 2014.

Hafner, P., McCarroll, D., Robertson, I., Loader, N. J., Gagen, M., Young, G. H., Bale, R. J., Sonninen, E. and Levanič, T.: A 520 year record of summer sunshine for the eastern European Alps based on stable carbon isotopes in larch tree rings, Clim Dyn, 43(3), 971–980, doi:10.1007/s00382-013-1864-z, 2014.

Hanel, M., Rakovec, O., Markonis, Y., Máca, P., Samaniego, L., Kyselý, J. and Kumar, R.: Revisiting the recent European droughts from a long-term perspective, Scientific Reports, 8(1), doi:10.1038/s41598-018-27464-4, 2018.

https://doi.org/10.5194/cp-2020-39
Preprint. Discussion started: 30 March 2020

Haupt, M., Weigl, M., Grabner, M. and Boettger, T.: A 400-year reconstruction of July relative air humidity for the Vienna region (eastern Austria) based on carbon and oxygen stable isotope ratios in tree-ring latewood cellulose of oaks (Quercus petraea Matt. Liebl.), Climatic Change, 105(1–2), 243–262, doi:10.1007/s10584-010-9862-1, 2011.

Heinrich, I., Touchan, R., Dorado Liñán, I., Vos, H. and Helle, G.: Winter-to-spring temperature dynamics in Turkey derived from tree rings since AD 1125, Climate Dynamics, 41(7–8), 1685–1701, doi:10.1007/s00382-013-1702-3, 2013.

Helama, S., Meriläinen, J. and Tuomenvirta, H.: Multicentennial megadrought in northern Europe coincided with a global El Niño–Southern Oscillation drought pattern during the Medieval Climate Anomaly, Geology, 37(2), 175–178, doi:10.1130/G25329A.1, 2009.

Helama, S., Läänelaid, A., Raisio, J., Mäkelä, H. M., Hilasvuori, E., Jungner, H. and Sonninen, E.: Oak decline analyzed using intraannual radial growth indices, δ13C series and climate data from a rural hemiboreal landscape in southwesternmost Finland, Environ Monit Assess, 186(8), 4697–4708, doi:10.1007/s10661-014-3731-8, 2014.

Helliker, B. R. and Griffiths, H.: Toward a plant-based proxy for the isotope ratio of atmospheric water vapor, Global Change Biology, 13(4), 723–733, doi:10.1111/j.1365-2486.2007.01325.x, 2007.

Hilasvuori, E., Berninger, F., Sonninen, E., Tuomenvirta, H. and Jungner, H.: Stability of climate signal in carbon and oxygen isotope records and ring width from Scots pine (Pinus sylvestris L.) in Finland, Journal of Quaternary Science, 24(5), 469–480, doi:10.1002/jqs.1260, 2009.

Hill, S. A., Waterhouse, J. S., Field, E. M., Switsur, V. R. and Rees, T. A.: Rapid recycling of triose phosphates in oak stem tissue, Plant, Cell & Environment, 18(8), 931–936, doi:10.1111/j.1365-3040.1995.tb00603.x, 1995.

Hirahara, S., Ishii, M. and Fukuda, Y.: Centennial-Scale Sea Surface Temperature Analysis and Its Uncertainty, Journal of Climate, 27(1), 57–75, doi:10.1175/JCLI-D-12-00837.1, 2014.

Hotelling, H.: The most predictable criterion, Journal of Educational Psychology, 26(2), 139–142, doi:10.1037/h0058165, 1935.

Ineson, S. and Scaife, A. A.: The role of the stratosphere in the European climate response to El Niño, Nature Geoscience, 2(1), 32–36, doi:10.1038/ngeo381, 2009.

Ionita, M., Tallaksen, L. M., Kingston, D. G., Stagge, J. H., Laaha, G., Van Lanen, H. A. J., Scholz, P., Chelcea, S. M. and Haslinger, K.: The European 2015 drought from a climatological perspective, Hydrology and Earth System Sciences, 21(3), 1397–1419, doi:10.5194/hess-21-1397-2017, 2017.

Josse, J. and Husson, F.: missMDA : A Package for Handling Missing Values in Multivariate Data Analysis, Journal of Statistical Software, 70(1), doi:10.18637/jss.v070.i01, 2016.

Kahmen, A., Sachse, D., Arndt, S. K., Tu, K. P., Farrington, H., Vitousek, P. M. and Dawson, T. E.: Cellulose δ18O is an index of leaf-to-air vapor pressure difference (VPD) in tropical plants, PNAS, 108(5), 1981–1986, doi:10.1073/pnas.1018906108, 2011.

Kaiser, H. F.: The Application of Electronic Computers to Factor Analysis:, Educational and Psychological Measurement, doi:10.1177/001316446002000116, 2016.

King, M. P., Yu, E. and Sillmann, J.: Impact of strong and extreme El Niños on European hydroclimate, Tellus A: Dynamic Meteorology and Oceanography, 72(1), 1–10, doi:10.1080/16000870.2019.1704342, 2020.

Labuhn, I., Daux, V., Pierre, M., Stievenard, M., Girardclos, O., Féron, A., Genty, D., Masson-Delmotte, V. and Mestre, O.: Tree age, site and climate controls on tree ring cellulose δ18O: A case study on oak trees from south-western France, Dendrochronologia, 32(1), 78–89, doi:10.1016/j.dendro.2013.11.001, 2014.

Labuhn, I., Daux, V., Girardclos, O., Stievenard, M., Pierre, M. and Masson-Delmotte, V.: French summer droughts since 1326 CE: a reconstruction based on tree ring cellulose delta O-18, Climate of the Past, 12(5), 1101–1117, doi:10.5194/cp-12-1101-2016, 2016.

Latif, M. and Grötzner, A.: The equatorial Atlantic oscillation and its response to ENSO, Climate Dynamics, 16(2–3), 213–218, doi:10.1007/s003820050014, 2000.

Li, J., Xie, S.-P., Cook, E. R., Huang, G., D'Arrigo, R., Liu, F., Ma, J. and Zheng, X.-T.: Interdecadal modulation of El Niño amplitude during the past millennium, Nature Climate Change, 1(2), 114–118, doi:10.1038/nclimate1086, 2011.

Lloyd-Hughes, B. and Saunders, M. A.: Seasonal prediction of European spring precipitation from El Niño–Southern Oscillation and Local sea-surface temperatures, International Journal of Climatology, 22(1), 1–14, doi:10.1002/joc.723, 2002.

Lorenz, E. N.: Empirical Orthogonal Functions and Statistical Weather Prediction, Massachusetts Institute of Technology, Department of Meteorology, Massachusetts., 1956.

Mathieu, P.-P., Sutton, R. T., Dong, B. and Collins, M.: Predictability of Winter Climate over the North Atlantic European Region during ENSO Events, J. Climate, 17(10), 1953–1974, doi:10.1175/1520-0442(2004)017<1953:POWCOT>2.0.CO;2, 2004.

McCarroll, D. and Loader, N. J.: Stable isotopes in tree rings, Quaternary Science Reviews, 23(7–8), 771–801, doi:10.1016/j.quascirev.2003.06.017, 2004.

Merkel, U. and Latif, M.: A high resolution AGCM study of the El Niño impact on the North Atlantic/European sector, Geophysical Research Letters, 29(9), 5-1-5–4, doi:10.1029/2001GL013726, 2002.

Nagavciuc, V., Ionita, M., Perşoiu, A., Popa, I., Loader, N. J. and McCarroll, D.: Stable oxygen isotopes in Romanian oak tree rings record summer droughts and associated large-scale circulation patterns over Europe, Clim Dyn, doi:10.1007/s00382-018-4530-7, 2018.

North, G. R., Bell, T. L., Cahalan, R. F. and Moeng, F. J.: Sampling Errors in the Estimation of Empirical Orthogonal Functions, Mon. Wea. Rev., 110(7), 699–706, doi:10.1175/1520-0493(1982)110<0699:SEITEO>2.0.CO;2, 1982.

Oikonomou, C., Flocas, H. A., Hatzaki, M., Nisantzi, A. and Asimakopoulos, D. N.: Relationship of extreme dry spells in Eastern Mediterranean with large-scale circulation, Theor Appl Climatol, 100(1), 137–151, doi:10.1007/s00704-009-0171-4, 2010.

van Oldenborgh, J. and Burgers, G.: Searching for decadal variations in ENSO precipitation teleconnections, Geophysical Research Letters, 32(15), doi:10.1029/2005GL023110, 2005.

Pearson, K.: On lines and planes of closest fit to systems of points in space, The London, Edinburgh, and Dublin Philosophical Magazine and Journal of Science, 2(11), 559–572, doi:10.1080/14786440109462720, 1902.

Pfahl, S. and Wernli, H.: Quantifying the relevance of atmospheric blocking for co-located temperature extremes in the Northern Hemisphere on (sub-)daily time scales, Geophysical Research Letters, 39(12), doi:10.1029/2012GL052261, 2012.

Porter, T. J., Pisaric, M. F. J., Field, R. D., Kokelj, S. V., Edwards, T. W. D., deMontigny, P., Healy, R. and LeGrande, A. N.: Spring-summer temperatures since AD 1780 reconstructed from stable oxygen isotope ratios in white spruce tree-rings from the Mackenzie Delta, northwestern Canada, Clim Dyn, 42(3–4), 771–785, doi:10.1007/s00382-013-1674-3, 2014.

Pozo-Vázquez, D., Esteban-Parra, M. J., Rodrigo, F. S. and Castro-Díez, Y.: The Association between ENSO and Winter Atmospheric Circulation and Temperature in the North Atlantic Region, Journal of Climate, 14(16), 3408–3420, doi:10.1175/1520-0442(2001)014<3408:TABEAW>2.0.CO;2, 2001.

Pozo-Vázquez, D., Gámiz-Fortis, S. R., Tovar-Pescador, J., Esteban-Parra, M. J. and Castro-Díez, Y.: El Niño–southern oscillation events and associated European winter precipitation anomalies, International Journal of Climatology, 25(1), 17–31, doi:10.1002/joc.1097, 2005.

https://doi.org/10.5194/cp-2020-39
Preprint. Discussion started: 30 March 2020

Rayner, N. A.: Global analyses of sea surface temperature, sea ice, and night marine air temperature since the late nineteenth century, Journal of Geophysical Research, 108(D14), doi:10.1029/2002JD002670, 2003.

Rimbu, N., Lohmann, G., Felis, T. and Tzold, J. P.: Shift in ENSO Teleconnections Recorded by a Northern Red Sea Coral, JOURNAL OF CLIMATE, 16, 9, 2003.

Rinne, K. T., Loader, N. J., Switsur, V. R. and Waterhouse, J. S.: 400-year May–August precipitation reconstruction for Southern England using oxygen isotopes in tree rings, Quaternary Science Reviews, 60, 13–25, doi:10.1016/j.quascirev.2012.10.048, 2013.

Roden, J. S., Lin, G. and Ehleringer, J. R.: A mechanistic model for interpretation of hydrogen and oxygen isotope ratios in tree-ring cellulose, Geochimica et Cosmochimica Acta, 64(1), 21–35, doi:10.1016/S0016-7037(99)00195-7, 2000.

Rozanski, K., Araguás-Araguás, L. and Gonfiantini, R.: Isotopic Patterns in Modern Global Precipitation, in Climate Change in Continental Isotopic Records, pp. 1–36, American Geophysical Union (AGU)., 2013.

Saurer, M., Borella, S., Schweingruber, F. and Siegwolf, R.: Stable carbon isotopes in tree rings of beech: climatic versus site-related influences, Trees, 11(5), 291, doi:10.1007/s004680050087, 1997.

Saurer, M., Cherubini, P., Reynolds-Henne, C. E., Treydte, K. S., Anderson, W. T. and Siegwolf, R. T. W.: An investigation of the common signal in tree ring stable isotope chronologies at temperate sites, Journal of Geophysical Research: Biogeosciences, 113(G4), doi:10.1029/2008JG000689, 2008.

Saurer, M., Kress, A., Leuenberger, M., Rinne, K. T., Treydte, K. S. and Siegwolf, R. T. W.: Influence of atmospheric circulation patterns on the oxygen isotope ratio of tree rings in the Alpine region, Journal of Geophysical Research: Atmospheres, 117(D5), doi:10.1029/2011JD016861, 2012.

Saurer, M., Spahni, R., Frank, D. C., Joos, F., Leuenberger, M., Loader, N. J., McCarroll, D., Gagen, M., Poulter, B., Siegwolf, R. T. W., Andreu-Hayles, L., Boettger, T., Liñán, I. D., Fairchild, I. J., Friedrich, M., Gutierrez, E., Haupt, M., Hilasvuori, E., Heinrich, I., Helle, G., Grudd, H., Jalkanen, R., Levanič, T., Linderholm, H. W., Robertson, I., Sonninen, E., Treydte, K., Waterhouse, J. S., Woodley, E. J., Wynn, P. M. and Young, G. H. F.: Spatial variability and temporal trends in water-use efficiency of European forests, Global Change Biology, 20(12), 3700–3712, doi:10.1111/gcb.12717, 2014.

Schleser, G. H., Frenzel, B., Stauffer, B. and Weiss, M. M.: Parameters determining carbon isotope ratios in plants, Problems of Stable Isotopes in Tree Rings, Lake Sediments and Peat Bogs as Climatic Evidence for the Holocene, Paläoklimaforschung 15, 71–95, 1995.

Schneider, U., Becker, A., Finger, P., Meyer-Christoffer, A., Ziese, M. and Rudolf, B.: GPCC's new land surface precipitation climatology based on quality-controlled in situ data and its role in quantifying the global water cycle, Theoretical and Applied Climatology, 115(1–2), 15–40, doi:10.1007/s00704-013-0860-x, 2014.

Schweingruber, F. H.: Tree Rings and Environment Dendroecology, Paul Haupt, Bern., 1996.

Seftigen, K., Linderholm, H. W., Drobyshev, I. and Niklasson, M.: Reconstructed drought variability in southeastern Sweden since the 1650s, International Journal of Climatology, 33(11), 2449–2458, doi:10.1002/joc.3592, 2013.

Siegmund, J. F., Siegmund, N. and Donner, R. V.: CoinCalc—A new R package for quantifying simultaneities of event series, Computers & Geosciences, 98, 64–72, doi:10.1016/j.cageo.2016.10.004, 2017.

Sillmann, J. and Croci-Maspoli, M.: Present and future atmospheric blocking and its impact on European mean and extreme climate, Geophysical Research Letters, 36(10), doi:10.1029/2009GL038259, 2009.

Sperry, J. S., Hacke, U. G. and Pittermann, J.: Size and function in conifer tracheids and angiosperm vessels, American Journal of Botany, 93(10), 1490–1500, doi:10.3732/ajb.93.10.1490, 2006.

Sternberg, L. and Deniro, M. J.: Isotopic Composition of Cellulose from C3, C4, and CAM Plants Growing Near One Another, Science, 220(4600), 947–949, doi:10.1126/science.220.4600.947, 1983.

Storch, H. v and Zwiers, F. W.: Statistical analysis in climate research, Cambridge University Press, Cambridge ; New York., 1999.

Tang, K. and Feng, X.: The effect of soil hydrology on the oxygen and hydrogen isotopic compositions of plants' source water, Earth and Planetary Science Letters, 185(3–4), 355–367, doi:10.1016/S0012-821X(00)00385-X, 2001.

Treydte, K., Schleser, G. H., Helle, G., Frank, D. C., Winiger, M., Haug, G. H. and Esper, J.: The twentieth century was the wettest period in northern Pakistan over the past millennium, Nature, 440(7088), 1179–1182, doi:10.1038/nature04743, 2006.

Treydte, K., Schleser, G. H., Esper, J., Andreu, L., Bednarz, Z. and Berninger, F.: Climate signals in the European isotope network ISONET, TRACE, 5, 138–147, 2007a.

Treydte, K., Frank, D., Esper, J., Andreu, L., Bednarz, Z., Berninger, F., Boettger, T., D'Alessandro, C. M., Etien, N., Filot, M., Grabner, M., Guillemin, M. T., Gutierrez, E., Haupt, M., Helle, G., Hilasvuori, E., Jungner, H., Kalela-Brundin, M., Krapiec, M., Leuenberger, M., Loader, N. J., Masson-Delmotte, V., Pazdur, A., Pawelczyk, S., Pierre, M., Planells, O., Pukiene, R., Reynolds-Henne, C. E., Rinne, K. T., Saracino, A., Saurer, M., Sonninen, E., Stievenard, M., Switsur, V. R.,

Szczepanek, M., Szychowska-Krapiec, E., Todaro, L., Waterhouse, J. S., Weigl, M. and Schleser, G. H.: Signal strength and climate calibration of a European tree-ring isotope network, Geophysical Research Letters, 34(24), doi:10.1029/2007GL031106, 2007b.

Treydte, K., Boda, S., Graf Pannatier, E., Fonti, P., Frank, D., Ullrich, B., Saurer, M., Siegwolf, R., Battipaglia, G., Werner, W. and Gessler, A.: Seasonal transfer of oxygen isotopes from precipitation and soil to the tree ring: source water versus needle water enrichment, New Phytologist, 202(3), 772–783, doi:10.1111/nph.12741, 2014.

Trouet, V., Babst, F. and Meko, M.: Recent enhanced high-summer North Atlantic Jet variability emerges from three-century context, Nature Communications, 9(1), doi:10.1038/s41467-017-02699-3, 2018.

Uppala, S. M., KÅllberg, P. W., Simmons, A. J., Andrae, U., Bechtold, V. D. C., Fiorino, M., Gibson, J. K., Haseler, J., Hernandez, A., Kelly, G. A., Li, X., Onogi, K., Saarinen, S., Sokka, N., Allan, R. P., Andersson, E., Arpe, K., Balmaseda, M. A., Beljaars, A. C. M., Berg, L. V. D., Bidlot, J., Bormann, N., Caires, S., Chevallier, F., Dethof, A., Dragosavac, M., Fisher, M., Fuentes, M., Hagemann, S., Hólm, E., Hoskins, B. J., Isaksen, L., Janssen, P. A. E. M., Jenne, R., Mcnally, A. P., Mahfouf, J.-F., Morcrette, J.-J., Rayner, N. A., Saunders, R. W., Simon, P., Sterl, A., Trenberth, K. E., Untch, A., Vasiljevic, D., Viterbo, P. and Woollen, J.: The ERA-40 re-analysis, Quarterly Journal of the Royal Meteorological Society, 131(612), 2961–3012, doi:10.1256/qj.04.176, 2005.

Vicente-Serrano, S. M., Beguería, S., López-Moreno, J. I., Angulo, M. and El Kenawy, A.: A New Global 0.5° Gridded Dataset (1901–2006) of a Multiscalar Drought Index: Comparison with Current Drought Index Datasets Based on the Palmer Drought Severity Index, Journal of Hydrometeorology, 11(4), 1033–1043, doi:10.1175/2010JHM1224.1, 2010.

Vitas, A.: Tree-Ring Chronology of Scots Pine (Pinus sylvestris L.) for Lithuania, BALTIC FORESTRY, 14(2), 6, 2008.

Wallace, J. M. and Gutzler, D. S.: Teleconnections in the Geopotential Height Field during the Northern Hemisphere Winter, Monthly Weather Review, 109(4), 784–812, doi:10.1175/1520-0493(1981)109<0784:TITGHF>2.0.CO;2, 1981.

Xoplaki, E., González-Rouco, J., Gyalistras, D., Luterbacher, J., Rickli, R. and Wanner, H.: Interannual summer air temperature variability over Greece and its connection to the large-scale atmospheric circulation and Mediterranean SSTs 1950–1999, Climate Dynamics, 20(5), 537–554, doi:10.1007/s00382-002-0291-3, 2003a.

Xoplaki, E., González-Rouco, J. F., Luterbacher, J. and Wanner, H.: Mediterranean summer air temperature variability and its connection to the large-scale atmospheric circulation and SSTs, Climate Dynamics, 20(7), 723–739, doi:10.1007/s00382-003-0304-x, 2003b.

https://doi.org/10.5194/cp-2020-39
Preprint. Discussion started: 30 March 2020

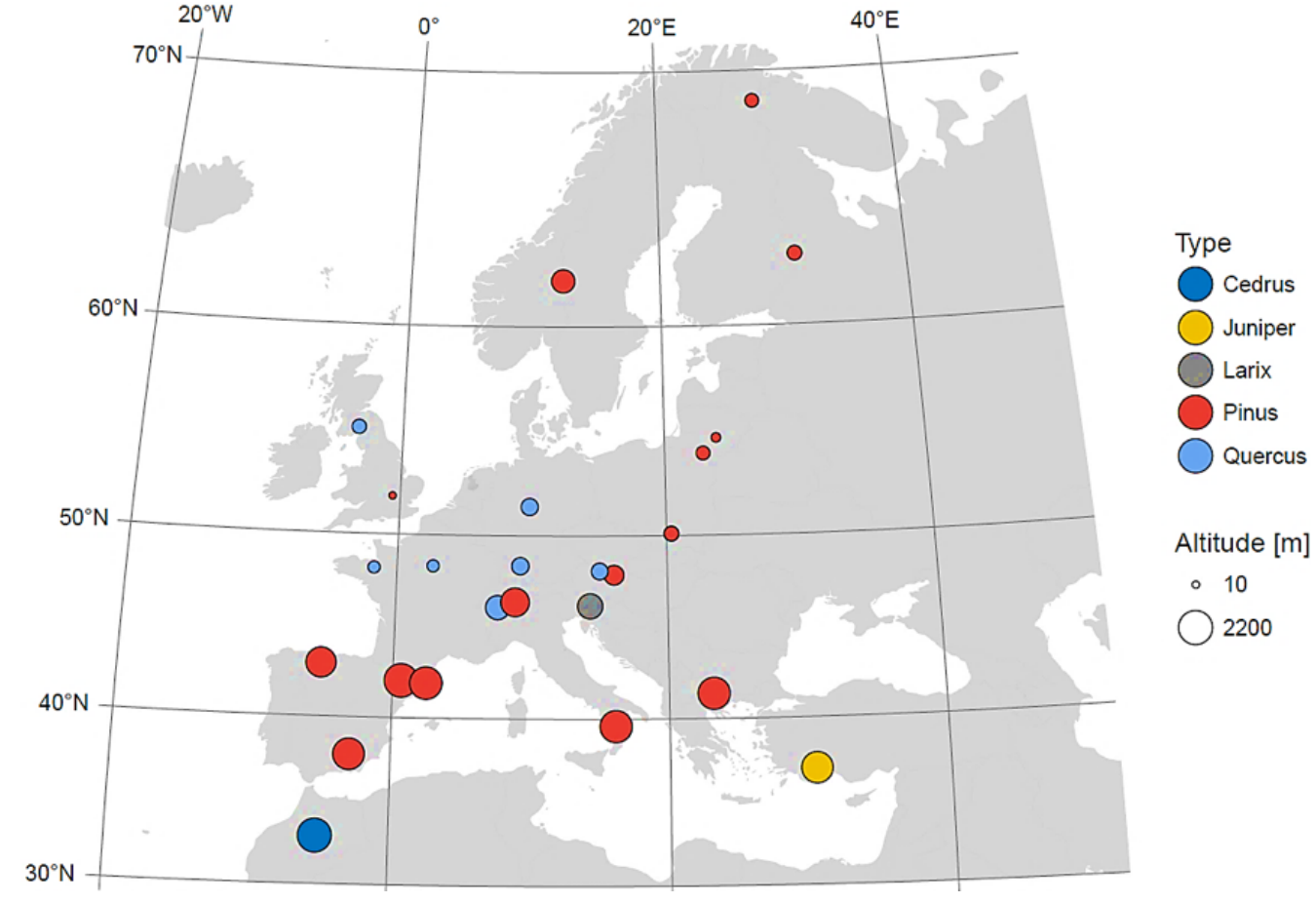

Figure 1: Spatial distribution of sample sites combined with the corresponding altitude. The highest density of sample sites exists in Central and Western Europe. The colour indicates the tree type (*Cedrus* (dark blue), *Juniper* (yellow), *Larix* (grey), *Pinus* (red) and *Quercus* (light blue)). The corresponding elevation (10-2200m) is shown by the size of the circles.

https://doi.org/10.5194/cp-2020-39
Preprint. Discussion started: 30 March 2020

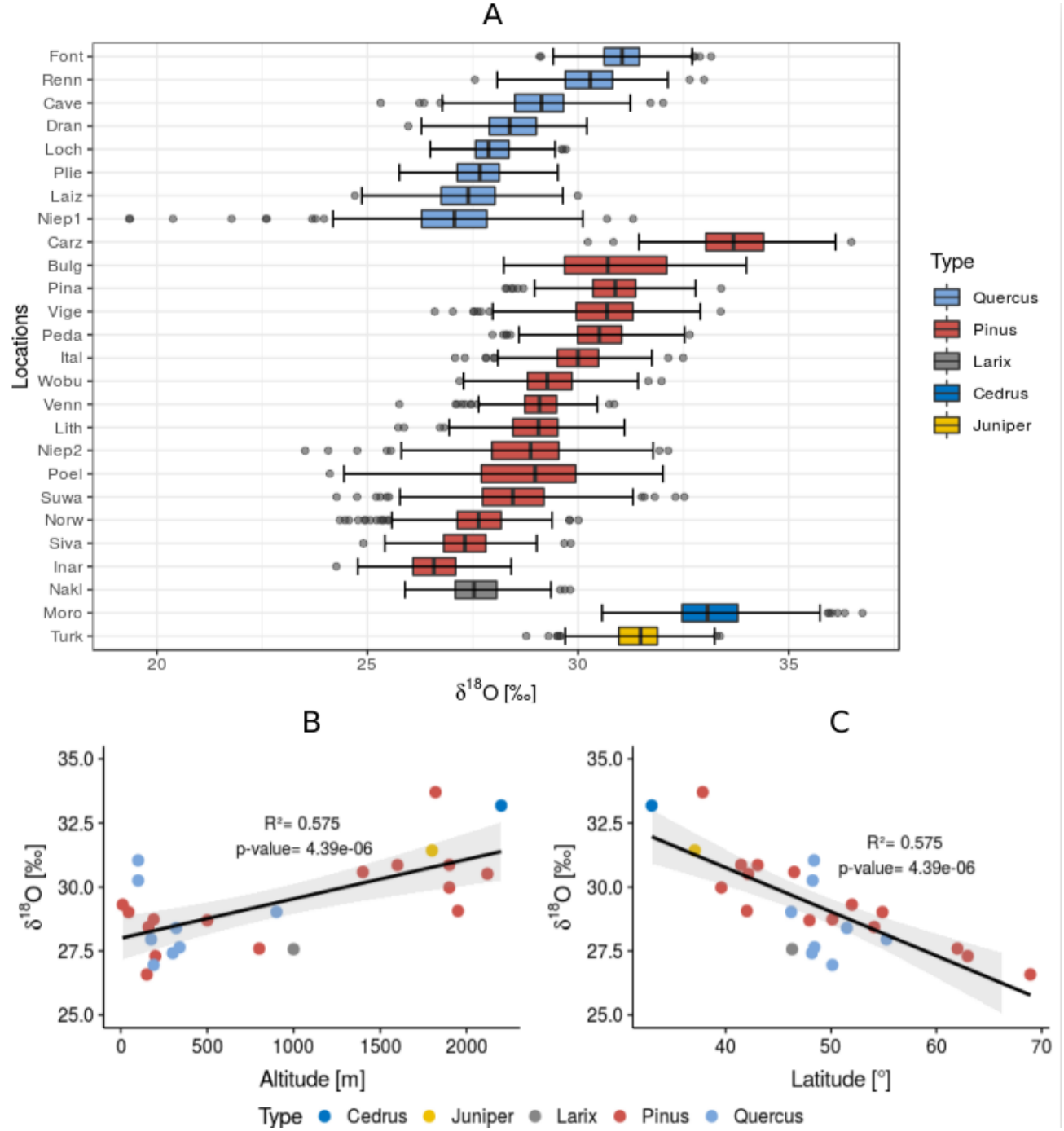

Figure 2: The characteristics of the European $\delta^{18}O$ time series/network. A, describes each time series with boxplots which were firstly ordered after the tree type and secondly after the average value. Additionally, the relation between the average value of each time series is plotted against their latitudinal (**B**) and their altitudinal position (**C**).

https://doi.org/10.5194/cp-2020-39
Preprint. Discussion started: 30 March 2020

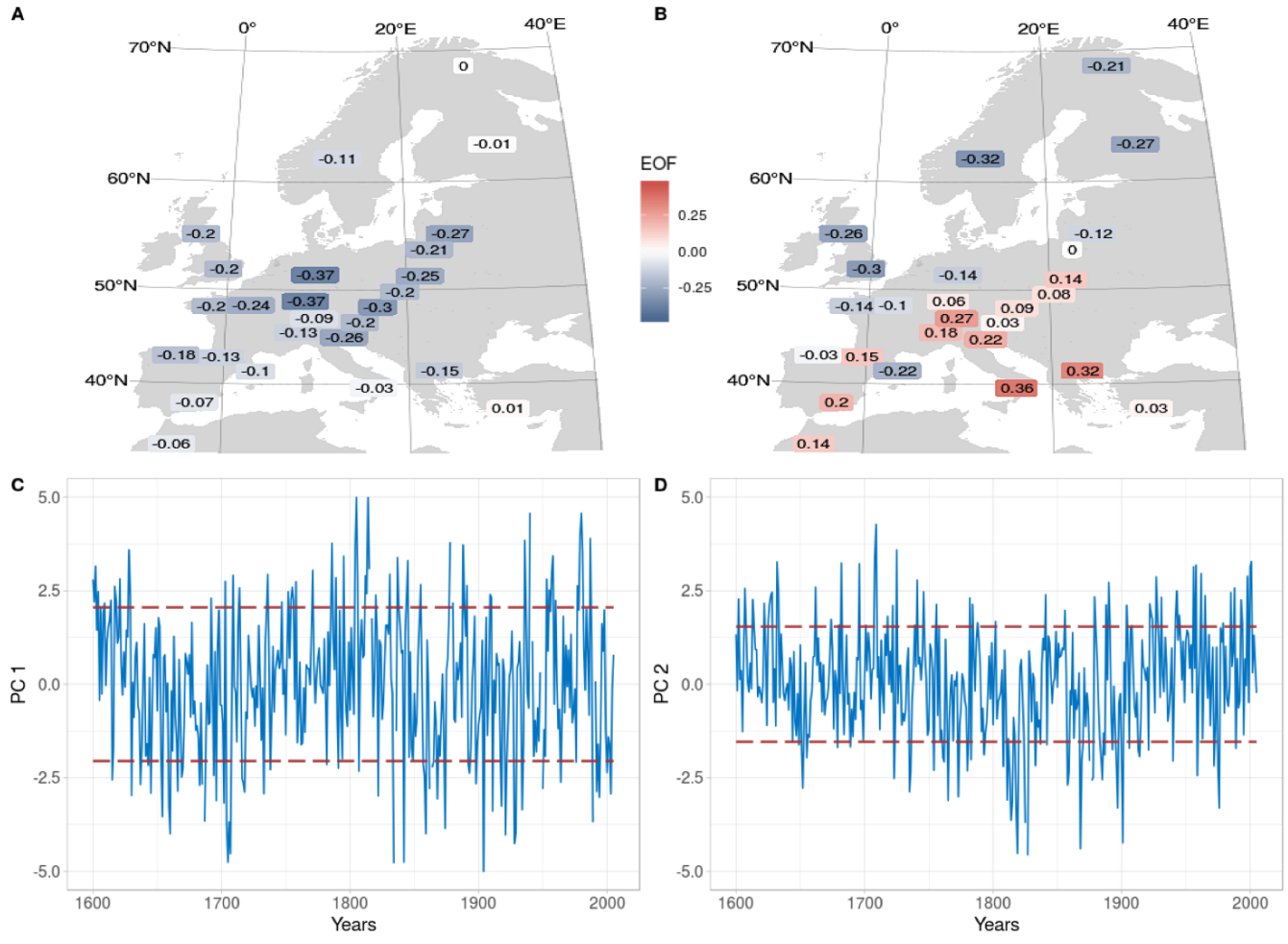

Figure 3: Spatial and temporal variability of the first two $\delta^{18}O$ components and EOFs. **A**, EOF for the first $\delta^{18}O$ component (16.2% explained variance), **B**, EOF for the second $\delta^{18}O$ component (9.5% explained variance). **C** and **D** are the time series for the first and second $\delta^{18}O$ component. The dashed red lines indicate the standard deviation for the years 1600-2005.

https://doi.org/10.5194/cp-2020-39
Preprint. Discussion started: 30 March 2020

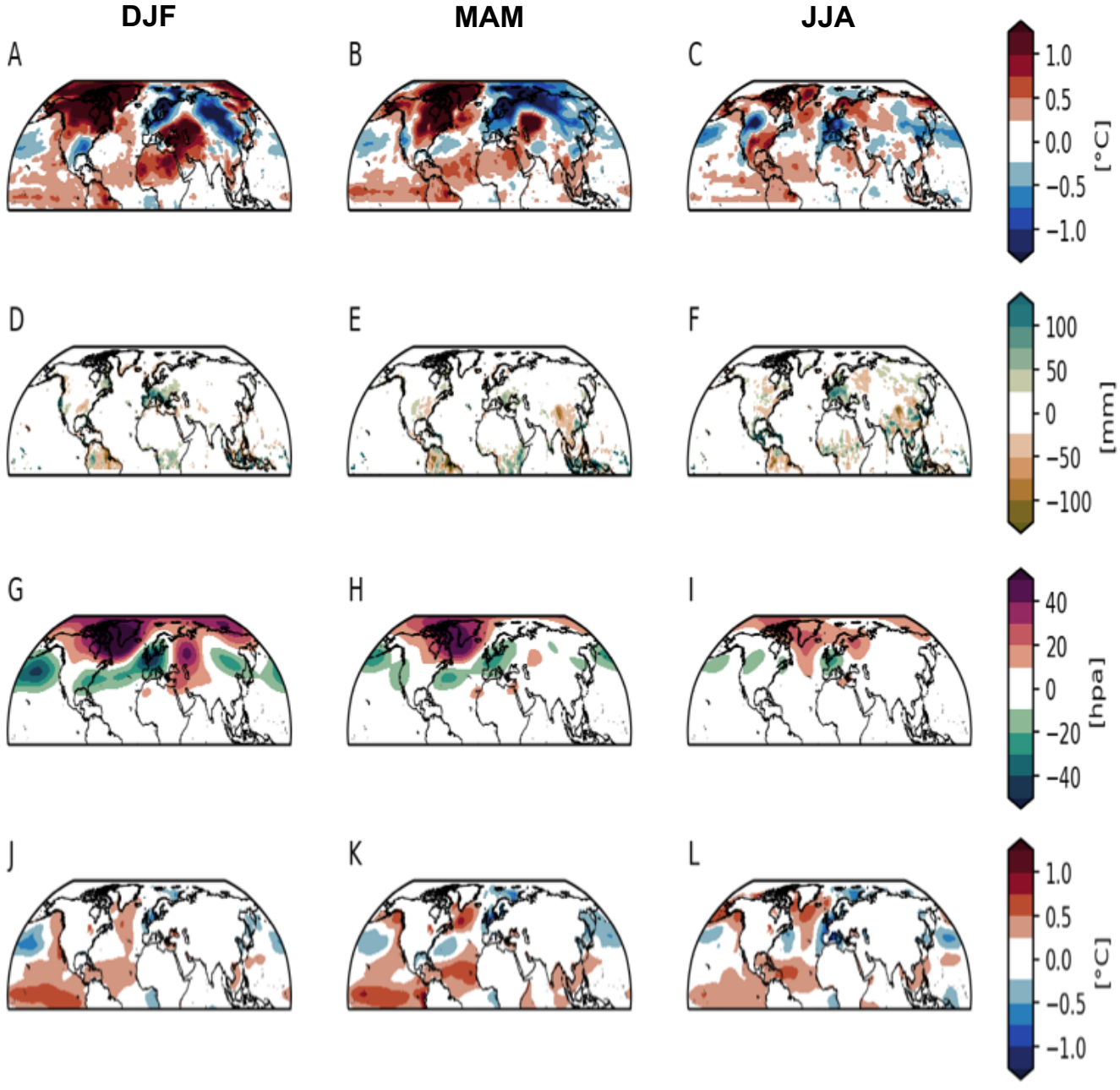

Figure 4: Composite maps (High-low) related to the first $\delta^{18}O$ component for the seasons DJF, MAM and JJA. The first row shows the characteristics of the climate in DJF, the second in MAM and the third row in JJA, whereas the first line shows the results for surface temperature, the second for precipitation, the third for Z500 and the fourth for SST. The Z500 maps show similar characteristics in winter and spring, whereas a pressure regime is directly located over Central Europe in summer. The SSTs in winter, spring and summer are characterized by ENSO activity. The Z500 and surface temperature dataset from 20CRv2c (Compo et al., 2011) and the COBE-SST2 dataset (Hirahara et al., 2014) are included in this Figure for the period 1851 to 2005 whereas the precipitation dataset from GPCC (Schneider et al., 2014) are used for the period 1901 to 2005.

https://doi.org/10.5194/cp-2020-39
Preprint. Discussion started: 30 March 2020

Climate of the Past
Discussions
Open Access
EGU

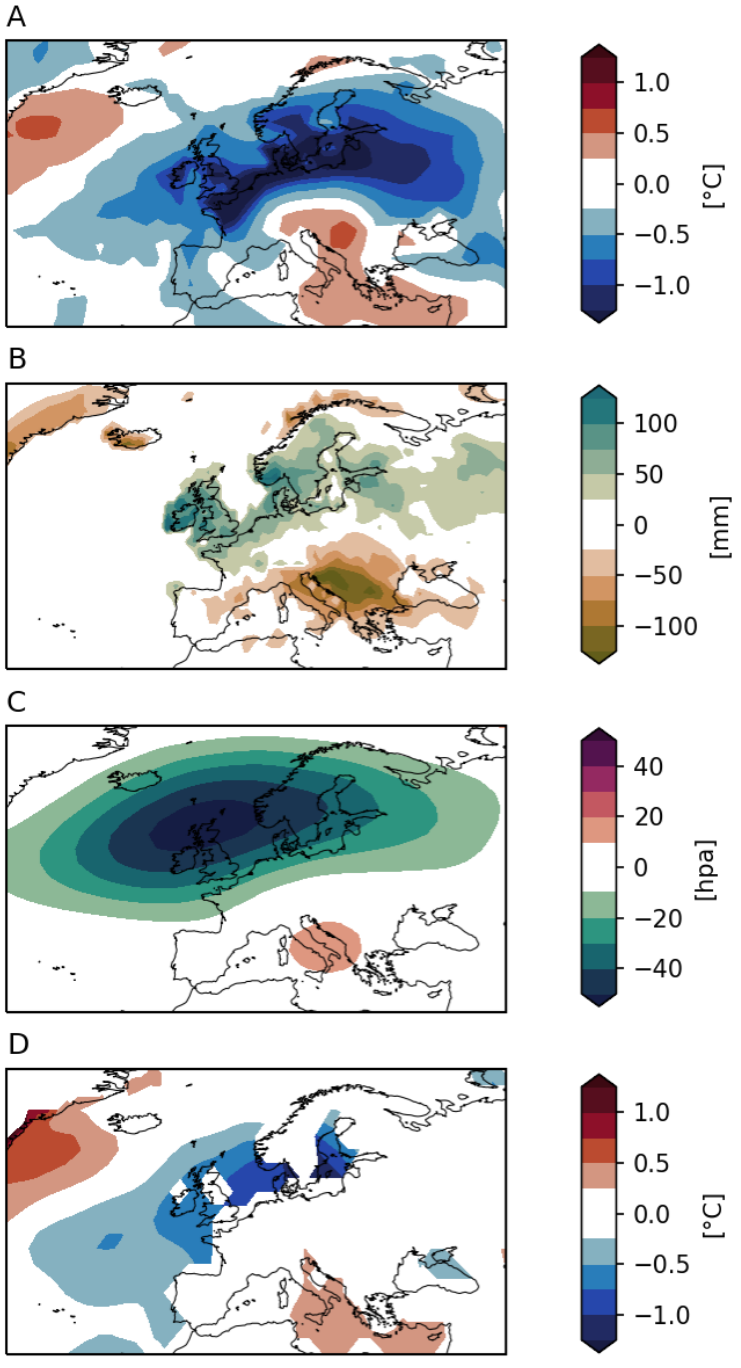

Figure 5: Composite maps (High-low) for the boreal summer related to the second $\delta^{18}O$ component. A, surface temperature JJA, **B,** precipitation JJA, **C,** Z500 JJA, **D,** SST JJA. The datasets are the same as in Figure 4.

https://doi.org/10.5194/cp-2020-39
Preprint. Discussion started: 30 March 2020

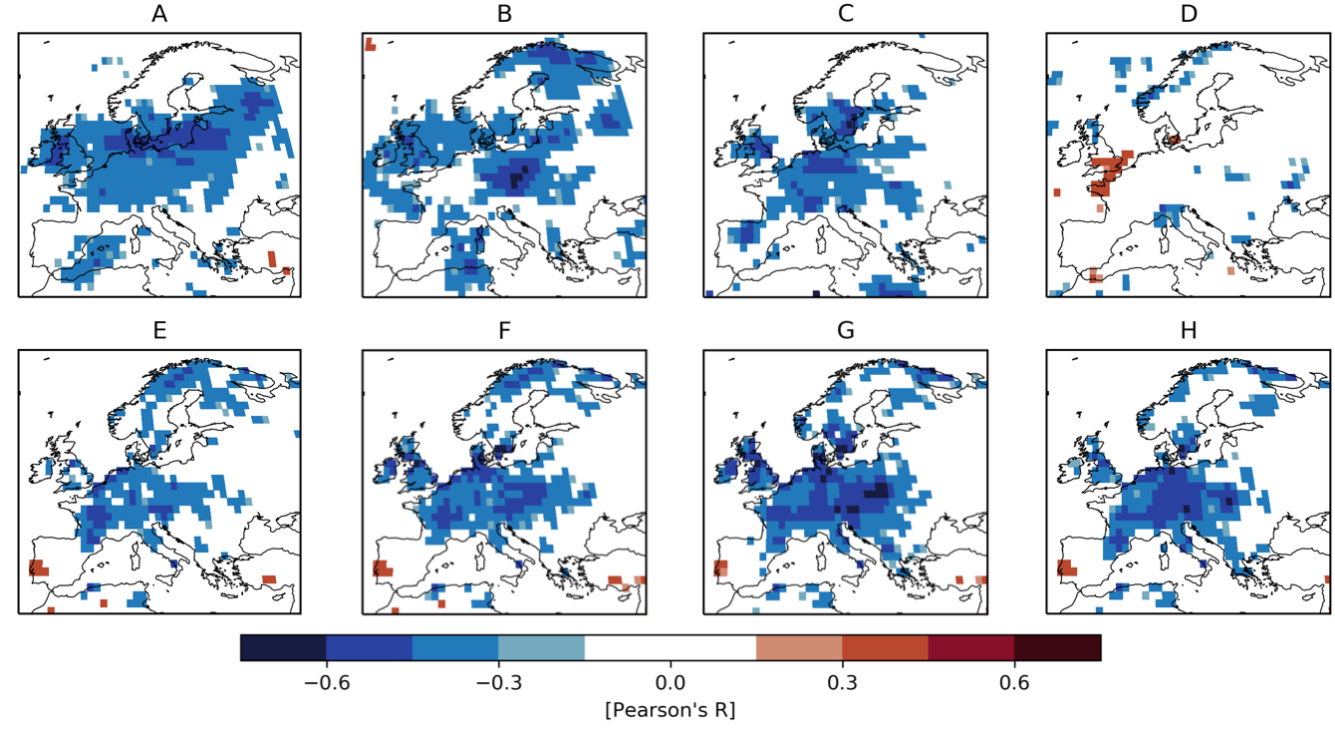

575 **Figure 6: Links between the first $\delta^{18}O$ component and the modelled $\delta^{18}O$ in soil water and precipitation from nudged climate simulations with ECHAM5-wiso (Butzin et al., 2014).** The upper line is showing the correlation between the first $\delta^{18}O$ component and $\delta^{18}O$ in precipitation for winter (A), spring (B), summer (C) and autumn (D). Figure E, F, G, H are the correlation maps for EOF1 and the$\delta^{18}O$ in soil water for winter, spring, summer and autumn. In all maps, the significant grid cells are coloured.

580